THE BELL SYSTEM TECHNICAL JOURNAL
Vol. 52, No. 10, December, 1973
Printed in U.S.A.

The Potential in a Charge-Coupled Device With No Mobile Minority Carriers

By J. McKENNA and N. L. SCHRYER

(Manuscript received May 17, 1973)

The potentials and fields in a two-dimensional model of a charge-coupled device (CCD) are studied. We assume no mobile minority carriers have been injected into the CCD and that the electrode voltages do not vary with time. The nonlinear equations describing the devices are first linearized using the depletion layer approximation. The linearized equations are then solved approximately by a fitting technique. Both surface and buried channel CCD's are considered. The accuracy and cost of obtaining the solution is discussed. This work is a continuation of a study initiated in an earlier paper.[1]

I. INTRODUCTION AND SUMMARY

In this paper we study the electrostatic potential distribution and fields in a two-dimensional model of a charge-coupled device[2,3] (CCD). This work is a continuation of a study initiated in an earlier paper[1] hereafter referred to as I. In I we considered a static, two-dimensional model with no mobile charge, and with electrodes so close together that they could be assumed to touch. We showed there that the depletion layer approximation[4] could be used to linearize the potential equations, and the linearized equations were then solved analytically. The numerical evaluation of these solutions was shown to be very accurate and cheap.

We extend the model of I to allow for gaps between the plates. Our purpose here is twofold. We want to examine the dependence of the potentials and fields in a CCD on various design parameters. As we show, our model allows considerable flexibility in describing various electrode configurations. In addition, however, we want to demonstrate a method of numerically solving the potential equations which we believe is of considerable interest in itself.

Both surface[2] and buried channel[5,6] CCD's are considered. However,

as in I, only the analysis for buried channel CCD's is given. The results for a surface CCD can be obtained as special cases of the results for buried channel CCD's. We refer the reader to I for a more detailed derivation of the equations and for a discussion of their linearization by the depletion layer approximation.

As we show by examples, fairly complicated models of CCD's can be analyzed at moderate cost by the methods of this paper. Nevertheless, the cost of using the methods of I to analyze a CCD with zero separation between the electrodes is typically an order of magnitude less than the cost of using the methods of this paper to analyze a CCD with nonzero electrode separation. This suggests that, in any complicated design problem, the methods of I should be used to rough out a solution, and then the solution should be "fine tuned" by using the methods of this paper. In addition, it is shown that, when the gaps between the electrodes are of the order of 1 μm, the potentials of interest are approximated well by the potentials in the same CCD with the electrode separation set to zero.

The nonlinear equations and boundary conditions defining the boundary value problem are introduced in Section II. The linearized equations are also introduced there. In Section III we discuss in some detail how we obtain approximate solutions to the linearized problem. The reader uninterested in the mathematical details should skip Section III and proceed directly to Section IV, which is devoted to examining some of the solutions with emphasis on how they are affected by changes in the design parameters. We examine a number of different design parameters, particularly for buried channel devices. The accuracy of the solutions and the cost of obtaining them is considered in Section V. Finally, some mathematical details are contained in two appendixes.

II. THE POTENTIAL EQUATIONS

We consider CCD's in which the minority carriers are holes and the underlying substrate is n-type silicon. The analysis can be modified in an obvious way to describe the case where the minority carriers are electrons and the substrate is p-type silicon.

A buried channel CCD consists of a substrate of n-type silicon on top of which there is a layer of p-type silicon. The p-type layer is covered with a layer of SiO_2, and closely spaced electrodes are placed on top of the oxide layer. A schematic diagram of such a device is shown in Fig. 1 with some typical dimensions indicated. A surface CCD is the same, except that the p-type layer is missing.

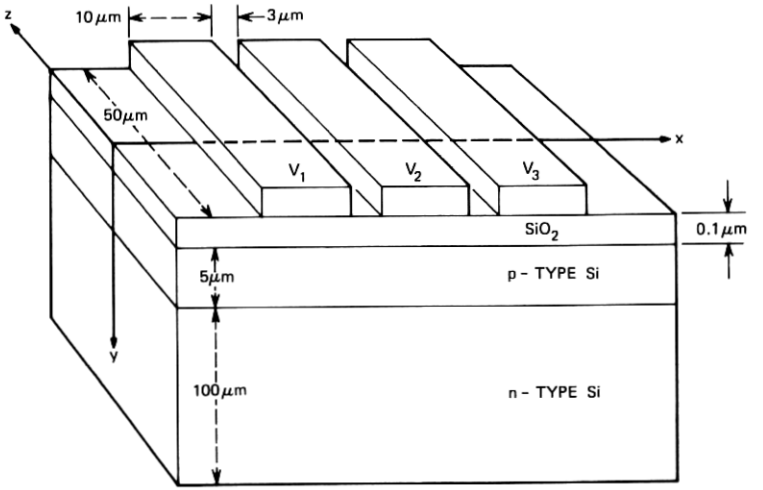

Fig. 1—A schematic diagram of a buried channel CCD.

We study here the static potential and fields in either a surface or buried channel CCD in the absence of mobile charge. Since the length in the z-direction of each plate is much greater than its width in the x-direction, near the center of the plates ($z=0$) the field is essentially two-dimensional; therefore, we treat the problem as two-dimensional.

We assume the bottom (n-type) substrate is infinitely thick. The field can penetrate into the substrate little beyond a depletion depth and, since for typical voltages the depletion depth ranges from 7 to 20 μm and the thickness of a typical device is 100 μm, this is a very good approximation.

It is assumed that there are gaps between the electrodes. We also make the approximation that the electrodes have zero thickness. Although this is a rather drastic simplification, we feel the essential effects of the gaps between the electrodes are still properly described. It will be seen later that electrodes of rectangular cross section could be studied, although at much greater cost. We further assume that the medium surrounding the electrodes has the same dielectric constant as the SiO_2. This is very reasonable, since in practice a CCD is covered with a dielectric coating. Two basic types of metalization are studied, single level and double level. In double-level metalization, two layers of electrodes are separated by an oxide layer. This is illustrated schematically in Fig. 2. We simulate this situation by assuming that the potential distribution in the gaps between the electrodes in the

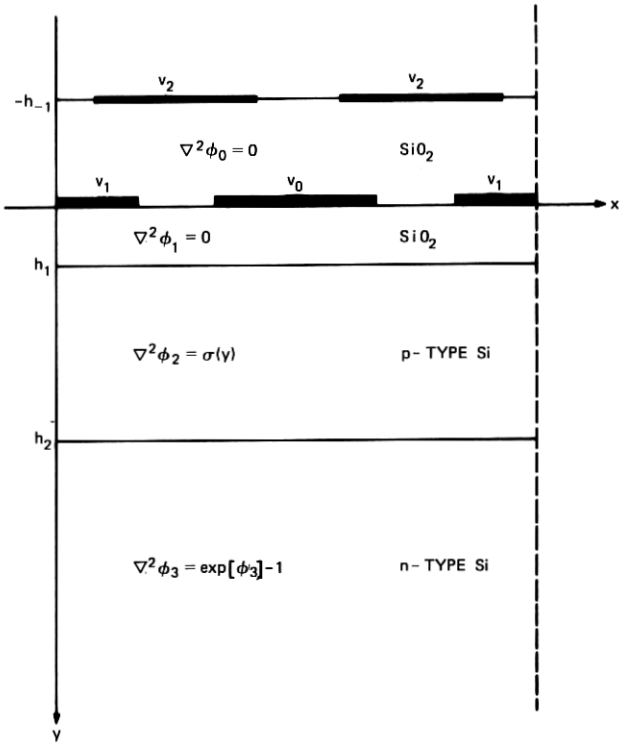

Fig. 2—A schematic diagram of one cell of a buried channel CCD with double-level metalization.

upper layer of electrodes is a known function. (Typically, the potential is assumed to vary piecewise linearly.) In single-level metalization, the upper level of electrodes is missing. Here we assume the dielectric coating over the electrodes is infinitely thick. Again, this is a reasonable assumption, since typically the field will have died out before reaching the surface of the dielectric coating.

Finally, we assume the structure to be periodic in the x-direction, which in the usual mode of operation is an excellent approximation.

The boundary value problem corresponding to our model of a buried channel CCD can be described by a system of partial differential equations which we wish to write in terms of dimensionless quantities. All dimensional quantities (measured in rationalized MKS units) will be starred, with the exception of a few obvious physical parameters. Corresponding unstarred quantities will be dimensionless. The physical parameters of the problem are ϵ_1 and ϵ_2, the permittivity of the oxide

and silicon, respectively; $-e$, the charge of an electron; Boltzman's constant k; the absolute temperature T; the length of a unit cell in the device L^*; the separation of the two layers of metalization h^*_{-1}; and h^*_1 and h^*_2, the thickness of the oxide layer and the p-layer, respectively. The donor number density of the n-type substrate is N^*_D, which in the usual method of fabricating a CCD is a constant. However, we assume the acceptor number density in the p-layer is given by the expression[7]

$$N^*_A(y^*) = C^*_s \exp\left\{-\left(\frac{y^* - h^*_1}{h^*_2 - h^*_1}\right)^2 \ell n \frac{C^*_s}{N^*_D}\right\} - N^*_D, \tag{1}$$

where C^*_s is the number density of acceptor ions at the upper surface of the Si.

Now define the (dimensional) Debye length λ_D,

$$\lambda = (\epsilon_2 \mathrm{k}T/e^2 N^*_D)^{\frac{1}{2}}. \tag{2}$$

Then the dimensionless lengths are defined as

$$x = x^*/\lambda_D, \quad y = y^*/\lambda_D, \quad L = L^*/\lambda_D, \quad h_\alpha = h^*_\alpha/\lambda_D, \quad (\alpha = \pm 1, 2). \tag{3}$$

The dimensionless potential is related to the dimensional potential by

$$\varphi(x, y) = e\varphi^*(x^*, y^*)/\mathrm{k}T. \tag{4}$$

If we set

$$C_s = C^*_s/N^*_D, \tag{5}$$

then the dimensionless p-layer acceptor density, $\sigma(y)$, is

$$\sigma(y) = C_s \exp\left\{-\left(\frac{y - h_1}{h_2 - h_1}\right)^2 \ell n\, C_s\right\} - 1. \tag{6}$$

In the strip $0 \leqq x \leqq L$, let φ_0 denote the electrostatic potential above the oxide layer, $-\infty < y \leqq 0$ in the case of single-level metalization and $-h_{-1} \leqq y \leqq 0$ in the case of double-layer metalization. Further, let φ_1 denote the potential in the oxide layer, $0 \leqq y \leqq h_1$; φ_2 the potential in the p-type layer, $h_1 \leqq y \leqq h_2$; and φ_3 the potential in the n-type substrate (see Fig. 2). Then in the dimensionless form, the potential equations are

$$\nabla^2\varphi_0 = 0, \qquad y \leqq 0, \tag{7}$$

$$\nabla^2\varphi_1 = 0, \qquad 0 \leqq y \leqq h_1, \tag{8}$$

$$\nabla^2\varphi_2 = \sigma(y), \qquad h_1 \leqq y \leqq h_2, \tag{9}$$

$$\nabla^2\varphi_3 = \exp(\varphi_3) - 1, \qquad h_2 \leqq y < \infty, \tag{10}$$

where ∇^2 is the two-dimensional Laplace operator. The standard

electromagnetic boundary conditions are as follows:

$$|\varphi_0(x, -\infty)| < \infty \text{ (single-level metalization), and} \tag{11}$$

$$\varphi_0(x, -h_{-1}) = U(x) \text{ (double-level metalization),} \tag{12}$$

where $U(x)$ is a given periodic function of period L, assuming on each electrode of the second level of metalization the constant voltage of the electrode and a specified potential between the electrodes. In reality, of course, the true potential in the gaps of the second level of metalization is unknown *a priori*. However, as indicated in Fig. 2, typically the semiconductor cannot "see" these gaps since they are shielded by the electrodes of the first level of metalization. Thus we simulate the exact boundary conditions in the gaps, most often by assuming the potential varies linearly from one electrode to another. We feel this is a good approximation, since we have performed calculations of the potential in the semiconductor with several different assumptions about the variation of the potential in the gaps, and the results were essentially identical. Further,

$$\varphi_0(x, 0) = V_j = \varphi_1(x, 0), \qquad (j = 1, 2, \cdots, p), \tag{13}$$

$$\varphi_0(x, 0) = \varphi_1(x, 0), \qquad \frac{\partial \varphi_0}{\partial y}(x, 0) = \frac{\partial \varphi_1}{\partial y}(x, 0) + \rho_g(x), \tag{14}$$

where V_j is the constant voltage of the jth electrode in the first level of metalization, eq. (13) holds on each of the p electrodes, and (14) holds in the gaps between the electrodes. Typically, $\rho_g(x) \equiv 0$, but in some cases it may describe a deliberately implanted surface charge in the gaps. In any event, $\rho_g(x)$ is a known function of x in the gaps, and $\rho_g(x) \equiv 0$ on the electrodes. Finally,

$$\varphi_1(x, h_1) = \varphi_2(x, h_1), \qquad \eta \frac{\partial \varphi_1}{\partial y}(x, h_1) = \frac{\partial \varphi_2}{\partial y}(x, h_1) + Q(x), \tag{15}$$

$$\varphi_2(x, h_2) = \varphi_3(x, h_2), \qquad \frac{\partial \varphi_2}{\partial y}(x, h_2) = \frac{\partial \varphi_3}{\partial y}(x, h_2), \tag{16}$$

$$\varphi_3(x, \infty) = 0, \tag{17}$$

and for all y

$$\varphi(0, y) = \varphi(L, y), \qquad \frac{\partial \varphi}{\partial x}(0, y) = \frac{\partial \varphi}{\partial x}(L, y). \tag{18}$$

In (15), $Q(x)$ is a known, periodic surface charge density, which may include deliberately implanted charges,[8] and

$$\eta = \epsilon_1/\epsilon_2. \tag{19}$$

All the boundary conditions (11) to (12) and (14) to (17) hold for $0 \leqq x \leqq L$.

The equations for the potential in a surface CCD are essentially the same, except the p-type layer is eliminated. We only give the analysis for the buried channel CCD. The results for the surface CCD can be obtained from those for the buried channel CCD by setting $\sigma(y) \equiv 0$, $h_1 = h_2$, and $\varphi_2 = \varphi_3$. In either case, the fields are obtained from the potential by

$$\mathbf{E} = -\nabla\varphi. \tag{20}$$

The results of I show that the system of eqs. (7) to (18) can be accurately solved by the method of finite differences only at great expense for even the simplest of devices. However, it was shown in I that, for the simpler problem studied there, the nonlinear boundary value problem could be replaced by a linear boundary value problem. This linear problem was solved analytically. It was then shown that under appropriate conditions the solution of the linear problem was an excellent approximation to the solution of the nonlinear problem in the p-type layer for a buried channel CCD and near the oxide-semiconductor interface for a surface CCD. The condition for the approximation to be a good one is, basically, that the potential along the line $y = h_2$ be large and negative. That condition holds in this problem, as we show later by example. Although the linear problem is much more complicated in this case because of the gaps between the electrodes and we have been unable to solve it analytically, we have been able to obtain good approximate solutions of it. For these reasons we now formulate the linear problem.

The linear equations are based on the depletion layer approximation, and we refer the reader to I and Ref. 4 for a detailed discussion. The linearization consists of replacing the single region $h_2 \leqq y < \infty$ by two regions, $h_2 \leqq y \leqq h_3 = h_2 + \hat{R}$ (the depletion layer) and $h_3 \leqq y < \infty$, and replacing the single nonlinear equation (10) by a different linear equation in each of these subregions (see Fig. 3).

$$\nabla^2\psi_0(x, y) = 0, \qquad y \leqq 0, \tag{21}$$

$$\nabla^2\psi_1(x, y) = 0, \qquad 0 \leqq y \leqq h_1, \tag{22}$$

$$\nabla^2\psi_2(x, y) = \sigma(y), \qquad h_1 \leqq y \leqq h_2, \tag{23}$$

$$\nabla^2\psi_3(x, y) = -1, \qquad h_2 \leqq y \leqq h_3 = h_2 + \hat{R}, \tag{24}$$

$$\nabla^2\psi_4(x, y) = \psi_4(x, y), \qquad h_3 \leqq y < \infty. \tag{25}$$

In addition to ψ_0, ψ_1, ψ_2, and ψ_3 satisfying boundary conditions (11) to

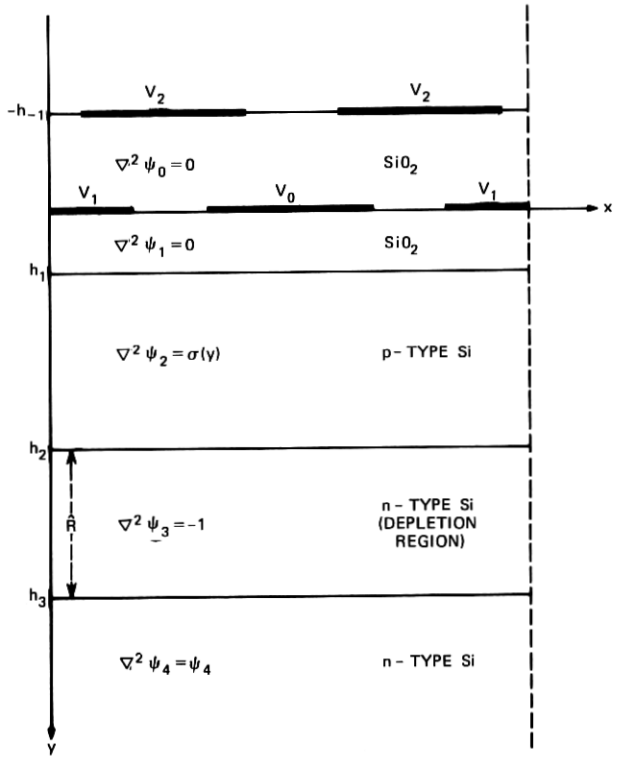

Fig. 3—A schematic diagram of the depletion layer approximation for one cell of a buried channel CCD with double-level metalization.

(16), we have the boundary conditions for $0 \leqq x \leqq L$

$$\psi_3(x, h_3) = \psi_4(x, h_3), \qquad \frac{\partial\psi_3}{\partial y}(x, h_3) = \frac{\partial\psi_4}{\partial y}(x, h_3), \tag{26}$$

$$\psi_4(x, \infty) = 0, \tag{27}$$

and the ψ_α, ($\alpha = 0, 1, 2, 3, 4$) all satisfy (18). The pseudodepletion depth $\hat{R}$ is best given by

$$\hat{R} = -\left(1 + h_2 - h_1 + \frac{h_1}{\eta}\right) + \left[\left(h_2 - h_1 + \frac{h_1}{\eta}\right)^2 - 1 - 2V - \frac{2h_1}{\eta}Q_{ss} + 2\int_{h_1}^{h_2}\left(\xi - h_1 + \frac{h_1}{\eta}\right)\sigma(\xi)d\xi\right]^{\frac{1}{2}}. \tag{28}$$

In (28),

$$Q_{ss} = \frac{1}{L}\int_0^L Q(x)dx$$

and V is the average electrode voltage. As shown in I and Ref. 4, ψ_0, ψ_1, and ψ_2 are quite insensitive to the choice of $\hat{R}$, and an optimal choice of $\hat{R}$ tends to minimize $\sup_{0 \leqq x \leqq L} |\psi_4(x, h_3) + 1|$.

III. SOLUTION OF THE LINEARIZED POTENTIAL EQUATIONS

The method we shall use to solve the linear system of elliptic eqs. (21) to (27) has much in common with previous work[9] on the classical problem of a single linear elliptic boundary value problem on a simply connected domain in the plane. The technique used in Ref. 9 is quite simple: Construct a family of particular solutions of the partial differential equation and, using a finite linear combination of these particular solutions, obtain a Chebyshev fit to the boundary conditions at a finite number of points on the boundary of the domain. It was shown that, as more and more particular solutions are taken in the linear combination and more and more points are chosen in the fit on the boundary, the linear combination converges to the true solution.

In this paper we construct a family of particular solutions of (21) to (27). These solutions depend linearly on a finite number N of parameters and satisfy *all* the boundary and interface conditions *except* that they do not assume the correct voltages on the electrodes at $y = 0$. We then complete the analogy with Ref. 9 by picking M points on the plates, x_i, $1 \leqq i \leqq M$, where $M \geqq N$, and force the potential to take on the correct value at the points x_i in the least-squares sense.

We obtain the family of particular solutions in the form of Fourier series. We assume as given the Fourier series expansions of $U(x)$ and $Q(x)$:

$$U(x) = \tfrac{1}{2}\alpha_0 + \sum_{n=1}^{\infty} G_n(x), \tag{29}$$

$$Q(x) = \tfrac{1}{2}\zeta_0 + \sum_{n=1}^{\infty} \Phi_n(x), \tag{30}$$

where

$$G_n(x) = \alpha_n \cos \lambda_n x + \beta_n \sin \lambda_n x, \tag{31}$$

$$\Phi_n(x) = \zeta_n \cos \lambda_n x + \xi_n \sin \lambda_n x, \tag{32}$$

and

$$\lambda_n = (2n\pi)/L. \tag{33}$$

Further, from I, we can write down formal expressions for ψ_1, ψ_2, ψ_3, and ψ_4 which satisfy (22) to (25) and boundary conditions (15), (16),

(18), (26), and (27). Let

$$F_n(x) = a_n \cos \lambda_n x + b_n \sin \lambda_n x, \tag{34}$$

$$E_\pm = 1 \pm 1/\eta, \tag{35}$$

$$\Lambda_n^\pm = 1 \pm (1 + \lambda_n^{-2})^{\frac{1}{2}}, \tag{36}$$

$$M_n(y) = \{E_+\Lambda_n^+ + E_-\Lambda_n^- e^{-2\lambda_n(h_3-h_1)}\}e^{-\lambda_n y} + \{E_-\Lambda_n^+ e^{-2\lambda_n h_1} + E_+\Lambda_n^- e^{-2\lambda_n h_3}\}e^{\lambda_n y}, \tag{37}$$

$$L_n(y) = 2\{\Lambda_n^+ e^{-\lambda_n y} + \Lambda_n^- e^{-\lambda_n(2h_3-y)}\}, \tag{38}$$

where η is given by (19), λ_n by (33), and a_0, a_n, b_n ($n = 1, 2, \cdots$) are unknown constants. Then these expressions are

$$\psi_1(x, y) = (A\bar{a}_0 + B) + (C\bar{a}_0 + D)y + \sum_{n=1}^{\infty} \left\{ F_n(x) \frac{M_n(y)}{M_n(0)} + \Phi_n(x) \frac{L_n(h_1)}{M_n(0)} \frac{\sinh \lambda_n y}{\eta\lambda_n} \right\}, \tag{39}$$

$$\psi_2(x, y) = \frac{1}{2}\left[\bar{a}_0(1 + h_3 - h_2) - (h_3 - h_2)^2 - (\bar{a}_0 + 2h_2 - 2h_3)(y - h_2) + 2\int_{h_2}^{y} (y - \xi)\sigma(\xi)d\xi\right] + \sum_{n=1}^{\infty} \left\{ F_n(x) + \Phi_n(x) \frac{\sinh \lambda_n h_1}{\eta\lambda_n} \right\} \frac{L_n(y)}{M_n(0)}, \tag{40}$$

$$\psi_3(x, y) = \tfrac{1}{2}[\bar{a}_0(1 + h_3 - y) - (y - h_3)^2] + \sum_{n=1}^{\infty} \left\{ F_n(x) + \Phi_n(x) \frac{\sinh \lambda_n h_1}{\eta\lambda_n} \right\} \frac{L_n(y)}{M_n(0)}, \tag{41}$$

$$\psi_4(x, y) = \tfrac{1}{2}\bar{a}_0 e^{-(y-h_3)} + 4\sum_{n=1}^{\infty} \left\{ F_n(x) + \Phi_n(x) \frac{\sinh \lambda_n h_1}{\eta\lambda_n} \right\} \cdot \frac{\exp\left[-\sqrt{1 + \lambda_n^2}(y - h_3) - \lambda_n h_3\right]}{M_n(0)}, \tag{42}$$

where

$$A = \frac{1}{2}\left(1 + h_3 - h_1 + \frac{h_1}{\eta}\right), \tag{43}$$

$$B = \int_{h_1}^{h_2} \left(\xi - h_1 + \frac{h_1}{\eta}\right)\sigma(\xi)d\xi - \frac{1}{2}\left[(h_3 - h_2)(h_3 + h_2 - 2h_1) + \frac{h_1}{\eta}(\zeta_0 + 2h_3 - 2h_2)\right], \tag{44}$$

$$C = -1/(2\eta), \tag{45}$$

$$D = \left[\zeta_0 + 2(h_3 - h_2) - 2\int_{h_1}^{h_2} \sigma(\xi)d\xi\right] \Big/ (2\eta), \tag{46}$$

and

$$\bar{a}_0 = (\tfrac{1}{2}a_0 - B)/A. \tag{47}$$

It should be noted that

$$\psi_1(x, 0) = \tfrac{1}{2}a_0 + \sum_{n=1}^{\infty} F_n(x). \tag{48}$$

In the case of single-level metalization we can write down an expression for a solution of (21) in $y \leqq 0$ which satisfies boundary conditions (11):

$$\psi_0(x) = \tfrac{1}{2}a_0 + \sum_{n=1}^{\infty} F_n(x)e^{\lambda_n y}. \tag{49}$$

In the case of double-level metalization, a solution of (21) in $-h_{-1} \leqq y \leqq 0$ satisfying boundary condition (12) is

$$\psi_0(x, y) = \frac{1}{2}\left(1 + \frac{y}{h_{-1}}\right)a_0 + \sum_{n=1}^{\infty} F_n(x)\frac{\sinh \lambda_n(y + h_{-1})}{\sinh \lambda_n h_{-1}} - \frac{\alpha_0}{2}\left(\frac{y}{h_{-1}}\right) - \sum_{n=1}^{\infty} G_n(x)\frac{\sinh \lambda_n y}{\sinh \lambda_n h_{-1}}. \tag{50}$$

Note that these solutions have been constructed so that from (48) and either (49) or (50), for $0 \leqq x \leqq L$,

$$\psi_0(x, 0) = \psi_1(x, 0). \tag{51}$$

[Note also that, term by term, (49) is the limit as $h_{-1} \to \infty$ of (50).]

Equations (34) to (50) contain expressions for ψ_α, $0 \leqq \alpha \leqq 4$, which satisfy the differential equations (21)–(25) and all the required boundary and interface conditions except condition (13) on the plates and the normal derivative condition of (14) in the gaps. These particular solutions contain the unknown parameters a_0, a_n, b_n, $(n = 1, 2, \cdots)$, which remain to be determined. At this point it might be assumed that the series should be truncated at some $n = N$ and the $2N + 1$ coefficients a_0, a_n, b_n, $n = 1, 2, \cdots, N$, be determined directly by making a least-squares fit to the remaining boundary conditions. However, it can be shown[10] that if $x_{j-1} < x_j$ are the end points of an electrode on $y = 0$ then for $x_{j-1} < x < x_j$, and x near x_j, say, $\partial\psi_0/\partial y(x, 0)$ will behave like $(x_j - x)^{-\frac{1}{2}}$ plus a power series in $(x_j - x)^{\frac{1}{2}}$. This implies that the Fourier series for $\psi_0(x, 0)$ converges very slowly. In fact, we have found that it is often necessary to take up to 2000 terms in the series to represent $\psi_0(x, 0)$ adequately. This makes it impractical to use the Fourier coefficients themselves as the parameters to be determined directly by a least-squares process.

Instead, we used the following technique. We approximated the charge density on $y = 0$ by a finite sum of known functions

$$\rho(x) = \rho_g(x) + \sum_{j=1}^{N} \rho_j p_j(x). \tag{52}$$

The functions $p_j(x)$ are zero except on the electrodes and are of several types, as shown in Fig. 4. The function $p_0(x)$ is a periodic, triangular spline for the ends of the device, as shown in Fig. 4a. Corresponding to the edge of each plate, there is a discontinuous triangular spline, Figs. 4b and 4c, and singular splines of the form $|x - x_k|^{-\frac{1}{2}}$, Figs. 4d and 4e. The remaining $p_j(x)$, whose supports lie wholly interior to the electrodes, are triangular splines as shown in Fig. 4f.

Now each unknown parameter a_0, a_n, b_n $(n = 1, 2, \cdots)$ is determined as a linear sum of the N parameters p_j, $1 \leqq j \leqq N$, by equating $\rho(x)$, given in (52) with $\partial\psi_0/\partial y(x, 0) - \partial\psi_1/\partial y(x, 0)$. In the case of single-level metalization, from (39) and (49),

$$\frac{\partial\psi_0}{\partial y}(x, 0) - \frac{\partial\psi_1}{\partial y}(x, 0) = -(C\bar{a}_0 + D) - \sum_{n=1}^{\infty} F_n(x)\lambda_n E_n - \sum_{n=1}^{\infty} \Phi_n(x) \frac{L_n(h_1)}{\eta M_n(0)}, \tag{53}$$

where

$$E_n = \frac{M_n'(0)}{\lambda_n M_n(0)} - 1. \tag{54}$$

It should be noted from (33), (35), (37), and (38) that, as $n \to \infty$,

$$E_n \approx -2, \qquad \frac{L_n(h_1)}{\eta M_n(0)} \approx \frac{2}{1 + \eta} e^{-\lambda_n h_1}. \tag{55}$$

In the case of double-level metalization, from (39) and (50),

$$\frac{\partial\psi_0}{\partial y}(x, 0) - \frac{\partial\psi_1}{\partial y}(x, 0) = \frac{a_0 - \alpha_0}{2h_{-1}} - (C\bar{a}_0 + D) - \sum_{n=1}^{\infty} F_n(x)\lambda_n H_n - \sum_{n=1}^{\infty} G_n(x) \frac{\lambda_n}{\sinh \lambda_n h_{-1}} - \sum_{n=1}^{\infty} \Phi_n(x) \frac{L_n(h_1)}{\eta M_n(0)}, \tag{56}$$

where

$$H_n = \frac{M_n'(0)}{\lambda_n M_n(0)} - \operatorname{ctnh}(\lambda_n h_{-1}). \tag{57}$$

It again follows from (33) and (37) that, as $n \to \infty$,

$$H_n \approx -2. \tag{58}$$

For a periodic function $f(x)$, of period L, we denote by $c_n[f]$ and

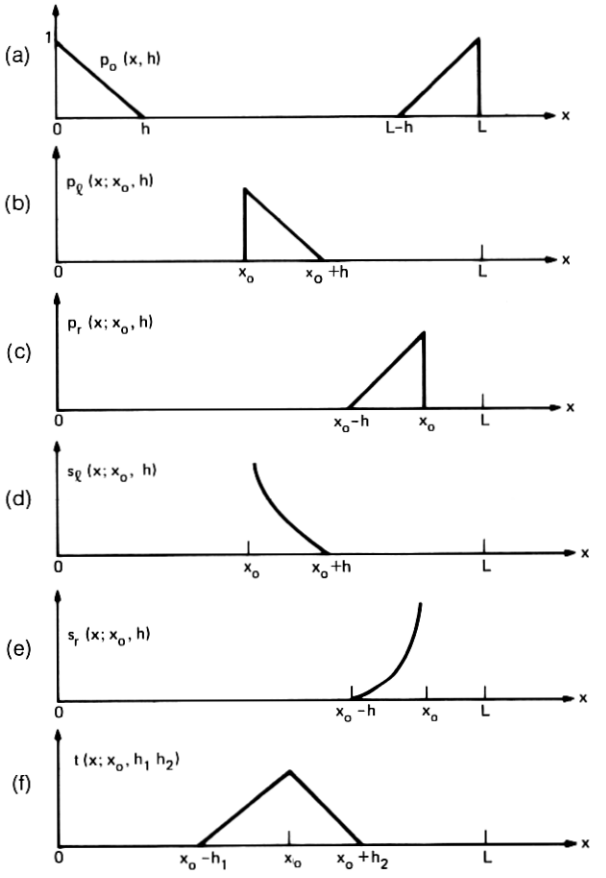

Fig. 4—The splines used to represent the charge density on the electrodes.

$s_n[f]$ the cosine and sine Fourier coefficients of f:

$$c_n[f] = \frac{2}{L}\int_0^L f(x)\cos(\lambda_n x)dx,\ s_n[f] = \frac{2}{L}\int_0^L f(x)\sin(\lambda_n x)dx. \quad (59)$$

Then, from (52), the Fourier series for $\rho(x)$ is

$$\rho(x) = \frac{1}{2}\left\{c_0[\rho_\varrho] + \sum_{j=1}^{N}\rho_j c_0[p_j]\right\} + \sum_{n=1}^{\infty}\left\{c_n[\rho_\varrho] + \sum_{j=1}^{N}\rho_j c_n[p_j]\right\}\cos\lambda_n x + \left\{s_n[\rho_\varrho] + \sum_{j=1}^{N}p_j s_n[p_j]\right\}\sin\lambda_n x. \quad (60)$$

In Appendix A we give $c_n[p_j]$ and $s_n[p_j]$ for the various functions $p_j(x)$. If we now equate (53) with (60), we can obtain the a_n and b_n as linear functions of the ρ_j in the case of single-level metalization:

$$a_0 = \frac{2(BC - AD)}{C} - \frac{A}{C}\left\{c_0[\rho_g] + \sum_{j=1}^{N} \rho_j c_0[p_j]\right\}, \tag{61}$$

$$a_n = -[\zeta_n L_n(h_1)]/[\eta\lambda_n E_n M_n(0)] - \left\{c_n[\rho_g] + \sum_{j=1}^{N} \rho_j c_n[p_j]\right\} \Big/ (\lambda_n E_n), \tag{62}$$

$$b_n = -[\xi_n L_n(h_1)]/[\eta\lambda_n E_n M_n(0)] - \left\{s_n[\rho_g] + \sum_{j=1}^{N} \rho_j s_n[p_j]\right\} \Big/ (\lambda_n E_n). \tag{63}$$

Similarly, if (56) is equated with (60), we obtain the a_n and b_n in the case of double-level metalization:

$$a_0 = \frac{2h_{-1}(BC - AD) - \alpha_0 A}{(h_{-1})C - A} - \frac{Ah_{-1}}{(h_{-1})C - A} \cdot \left\{c_0[\rho_g] + \sum_{j=1}^{N} \rho_j c_0[p_j]\right\}, \tag{64}$$

$$a_n = -\frac{\alpha_n}{H_n \sinh(h_{-1}\lambda_n)} - \frac{\zeta_n L_n(h_1)}{\eta\lambda_n H_n M_n(0)} - \left\{c_n[\rho_g] + \sum_{j=1}^{N} p_j c_n[p_j]\right\} \Big/ (\lambda_n H_n), \tag{65}$$

$$b_n = -\frac{\beta_n}{H_n \sinh(h_{-1}\lambda_n)} - \frac{\xi_n L_n(h_1)}{\eta\lambda_n H_n M_n(0)} - \left\{s_n[\rho_g] + \sum_{j=1}^{N} \rho_j s_n[p_j]\right\} \Big/ (\lambda_n H_n). \tag{66}$$

Equations (39) to (42) and either (49) or (50), with the a_n and b_n defined by eqs. (61) to (63) or (64) to (66), respectively, define solutions to eqs. (21) to (25) which satisfy boundary conditions (11) or (12), (14) to (16), (26), and (27). They do not, however, assume the correct values on the electrodes at $y = 0$; i.e., (13) is not satisfied. These solutions depend linearly on the N unknown constants ρ_j, $1 \leqq j \leqq N$, and of course on the choice of functions $p_j(x)$ used to describe the charge density on the plates. Having picked the $p_j(x)$ described earlier, M_j points are chosen on the jth electrode, $x_i^{(j)}$, $1 \leqq i \leqq M_j$, with

$$M = \sum_{j=1}^{p} M_j \geqq N.$$

Then the expression

$$\sum_{j=1}^{p} \sum_{i=1}^{M_j} [\psi_0(x_i^{(j)}, 0) - V_j]^2 \tag{67}$$

is minimized with respect to the ρ_α.

It has been observed that near the edge of an electrode, where the potential has square-root behavior, the fitting points $x_i^{(j)}$ should be spaced quadratically closer together as the edge of the electrode is approached. If $x = e$ is an edge of the jth plate, then we distributed the points near this edge by picking $b \neq e$ and an integer $m < M_j/2$ and setting

$$z_j = b + (e - b) \cos \frac{(j - 1)\pi}{2(m - 1)}, \qquad (1 \leqq j \leqq m). \tag{68}$$

The points z_j were then used as the fitting points x_i near the edge of the plate. Away from the edges of the plate, the fitting points were uniformly distributed.

We have assumed the existence of a bounded solution $\psi(x, y)$ to the linearized problem. In Appendix B we show that if $\psi(x, y)$ is the true solution of the linearized problem and $\psi^a(x, y)$ is one of our approximate solutions, then the error $\psi(x, y) - \psi^a(x, y)$ is bounded at every point by the maximum error on the electrodes. Since the true solution is known on the electrodes, this provides us with *a posteriori* error bounds. We will make use of this important point later in evaluating the quality of our approximate solutions.

The technique described in this section can be formulated in a rather general setting and, we believe, can be applied to many problems of interest in physics and engineering. It has been used by Morrison et al. in a study of microwave scattering by deformed raindrops.[11] Assume that a problem can be separated into two parts: Input data and a governing system of partial differential equations (PDE's), with possible interface conditions, which determine the solution when given the input data. Further, assume that linear families of particular solutions to the PDE's can be found. For example, these may be constructed by separation of variables, Fourier series, Green's Theorems, etc. Finally, assume that by linearly parameterizing some unknowns of the solution (for our problem, the charge distribution on the plates) we can obtain particular solutions to both the PDE's and the interface conditions. Then one could use some fitting procedure, a discrete least-squares fit, for example, to force the linear family of particular solutions to the governing system to have approximately the same

input data as the desired solution. This generates a solution of exactly the same governing system, but with input data which differs by a known, and hopefully small, amount from the desired input data. For all practical purposes, this gives an effective bound on the error in the computed approximate solution. For example, if the desired input is only known to 1 percent, because of experimental error in measuring it, then any solution generated by the above procedure which corresponds to the desired input data perturbed by at most 1 percent cannot, on the basis of comparing inputs, be distinguished from the true solution of the problem.

Also, in many cases, one can use the Maximum Principle, conservation of energy, or some other basic principle to give sharp, rigorous bounds on the error in such an approximate solution in terms of how well it satisfies the given input data. We do this for our problem in Appendix B. This is a very great improvement over the standard discretization methods for solving such problems. Those methods generally give an approximate solution to an approximate system of equations, but with exactly the given input data, with the result that it is very difficult to estimate reliably what the true error is for a given approximate solution.

IV. THE POTENTIALS AND FIELDS IN SOME SPECIFIC CCD'S

Using the method described in Section III, we have evaluated approximately the solutions of eqs. (21) to (25) for a number of different plate configurations and design parameters, and we present some of these results graphically in this section.

We have assumed in each case that the n-type substrate doping is $N_D^* = 10^{14}$ cm^{-3}, that $\epsilon_2/\epsilon_0 = 12$, where ϵ_0 is the permittivity of free space, that $\epsilon_1/\epsilon_2 = \frac{1}{3}$, and that $Q(x) \equiv 0$, i.e., there is no trapped or implanted charge at the oxide-semiconductor interface. Then at $T = 300°$K, the Debye length is $\lambda_0 = 0.415$ μm. In addition, we have used the factor $(kT/e) = 0.025$ V to convert dimensionless potentials to volts, and the factor $(kT/e\lambda_D) = 600$ V/cm to convert dimensionless fields to volts per centimeter. In each example involving a buried channel CCD, we assume that the acceptor number density in the p-layer is given by (1), [(6)] with $C_s^* = 4.6 \times 10^{15}$ cm^{-3} [$C_s = 46$]. In each such case, this corresponds to an average number density of acceptor atoms of 2×10^{15} cm^{-3} [see eq. (2.5) of I].

In I we investigated the effects of changing the p-layer doping and thickness, and so here we concentrate mainly on the effects of gap width, plate potential, and the separation of the levels of metalization.

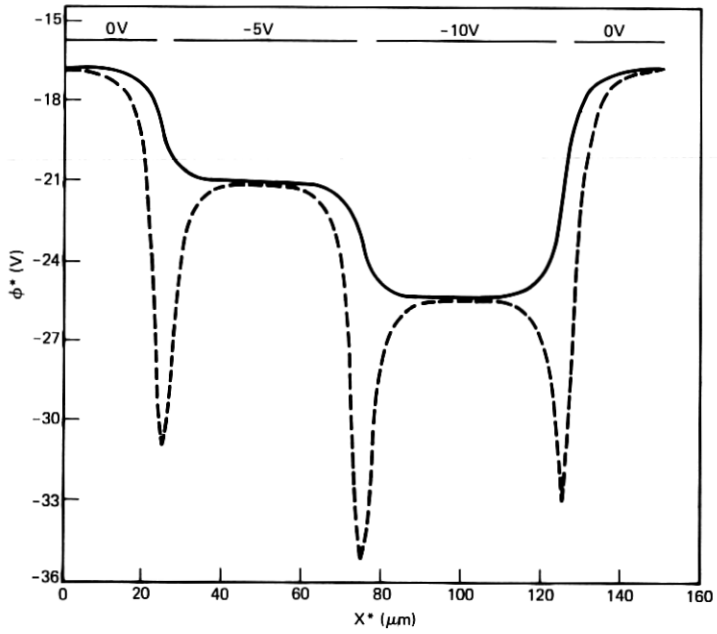

Fig. 5—The channel potential φ^* plotted as a function of x^* for a three-phase buried channel CCD. The 45-μm-wide electrodes are at 0, -5, and -10 V; the gaps are 5 μm wide; $h_1^* = 0.1$ μm; $h_2^* - h_1^* = 5$ μm; and $C_s^* = 4.6 \times 10^{15}$ cm^{-3}. The dashed curve is for no surface charge implanted in the gaps; the solid curve is for $\rho_g^*/e = 0.8 \times 10^{12}$ cm^{-2} implanted in the gaps.

In Figs. 5 and 6 we show some properties of a three-phase buried channel CCD with single-level metalization. The electrodes are 45 μm wide, and the gaps between them are 5 μm wide. The p-layer is 5 μm thick ($h_2^* - h_1^* = 5$ μm), and the oxide layer is 0.1 μm thick ($h_1^* = 0.1$ μm). The region $y < 0$ is assumed to be filled with SiO_2. The potentials on the electrodes are 0, -5, and -10 V, as shown. The dashed curve in Fig. 5 shows the channel potential φ^* (that is, the value of the potential at the potential minimum in the p-layer) as a function of x^* when there is no implanted surface charge in the gaps between electrodes $[\rho_g^*(x^*) \equiv 0]$. This curve illustrates one early difficulty encountered in the design of buried channel CCD's, namely the large potential well under the gap between the plates. A CCD with almost these same parameters was constructed[5] and did not work because of the variable amounts of charge trapped in these wells. In the remainder of this section we discuss a number of possible methods of eliminating this potential well in the gaps between the plates.

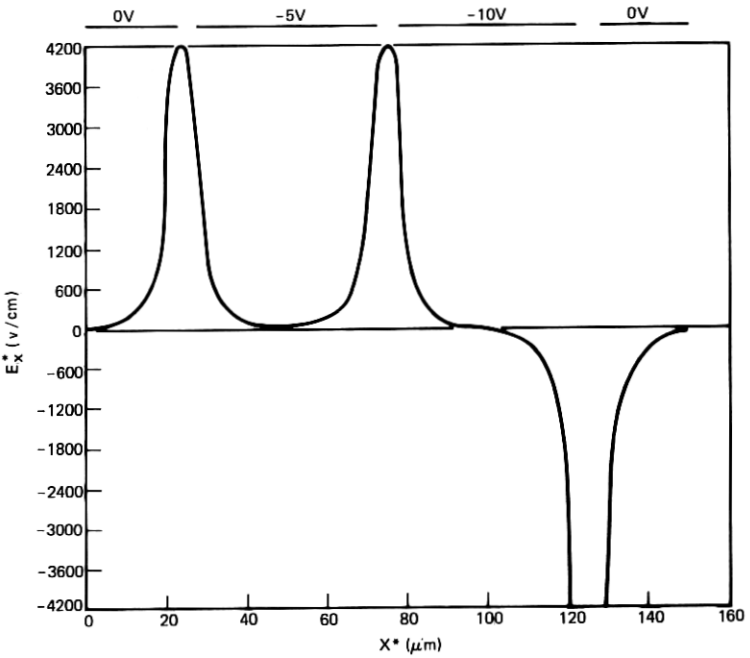

Fig. 6—The channel field $-\partial\varphi^*/\partial x^*$ plotted as a function of x^* for the CCD of Fig. 5 with $\rho_g^*/e = 0.8 \times 10^{12}$ cm^{-2} implanted in the gaps.

An operating buried channel CCD has been reported[12] in which the gaps between the electrodes have been filled with a resistive material so that the potential drop between the electrodes is essentially linear. This CCD was also discussed in I, and it was shown there that the potential wells are eliminated. Another technique for eliminating the potential wells is to implant a layer of positive surface charge in the gap between the electrodes. (Other schemes for eliminating this problem are discussed in the literature.[13]) The solid curve in Fig. 5 shows the channel potential in the same three-phase CCD after a uniform surface charge density, $\rho_g^*(x^*)/e = 0.8 \times 10^{12}$ cm^{-2} $[\rho_g(x) = 578]$, has been implanted in the gaps between the electrodes. Note that

$$\int_{h1}^{h2} N_A^*(y^*)dy^* = 10^{12} \text{ cm}^{-2}.$$

This technique should also eliminate the potential wells under the gaps. In Fig. 6 we plot the channel field $E_x^* = -\partial\varphi^*/\partial x^*$ (that is, the field at the potential minimum in the p-layer) as a function of x^*.

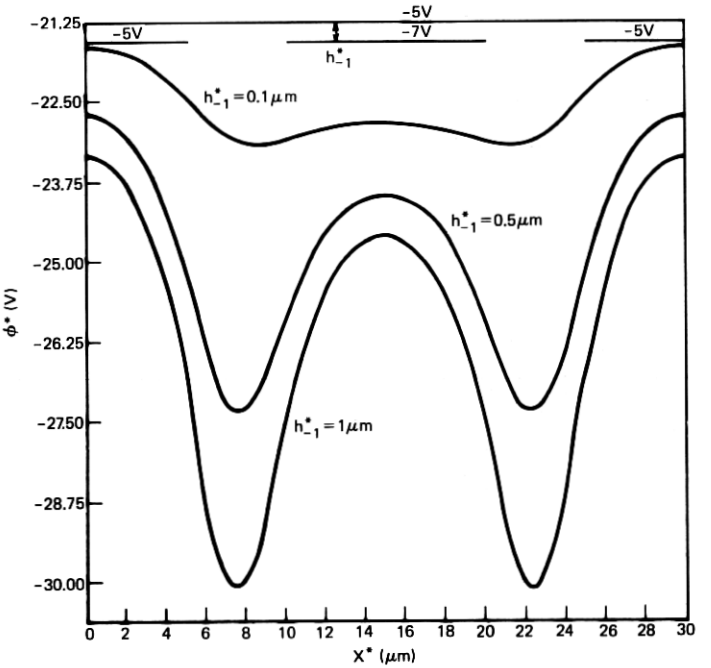

Fig. 7—The channel potential in a buried channel CCD with double-level metalization. The lower level electrodes are 10 μm wide with 5-μm gaps and are at potentials of -5 and -7 V. The upper level is a single electrode at -5 V; $h_1^* = 0.1$ μm; $h_2^* - h_1^* = 5$ μm; $C_i^* = 4.6 \times 10^{15}$ cm^{-3}; and the separation of the metalization levels is $h_{-1}^* = 0.1$, 0.5, and 1.0 μm.

This shows that there are substantial fields in the gap between the -5 and -7 V electrodes, but the field penetration under the electrodes is not too good.

In Figs. 7 to 9 we investigate the possibility of eliminating the potential wells by the use of double-level metalization, in which the upper level of metal is a single continuous piece covering the entire channel and has a dc potential applied to it. The presence or absence of the potential wells is mainly a local phenomenon and can be studied by considering just two adjacent electrodes in the lower level of metalization. Thus, in the interests of economy we consider a model CCD in which alternate electrodes of the lower level are at the same voltage. These plates are 10 μm wide and the gaps between them are 5 μm wide. The oxide layer between the first level of electrodes and the p-layer is 0.1 μm thick ($h_1^* = 0.1$ μm) and the p-layer is 5 μm thick ($h_2^* - h_1^* = 5$ μm). For the CCD of Fig. 7, the electrodes on the lower

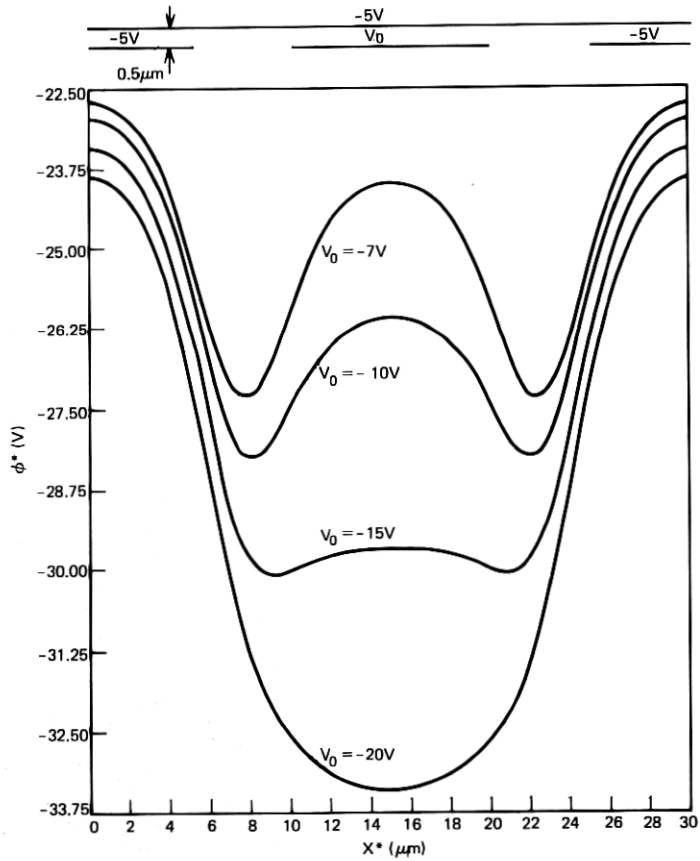

Fig. 8—The channel potential in the CCD of Fig. 7 with the separation of the metalization levels held fixed at $h^*_{-1} = 0.5$ μm and the potential of the center, lower-level electrode taking the values −7, −10, −15, and −20 V.

level are at a potential of −5 and −7 V, and the upper level consists of a single electrode, covering the whole device, which is at a potential of −5 V. In Fig. 7 we plot the channel potential for three different separations of the levels of metalization, $h^*_{-1} = 0.1$, 0.5, and 1 μm. Even with $h^*_{-1} = 0.1$ μm, there is still a very slight well in the gaps.

We next see what happens if we hold the separation of the levels of metalization at $h^*_{-1} = 0.5$ μ and change the voltage, v_0, on the middle electrode in the lower level. In Fig. 8 we plot the resulting channel potential, φ^*, as a function of x^* for $v_0 = -7$, −10, −15, and −20 V. From these graphs we see that a potential difference of 15 V between

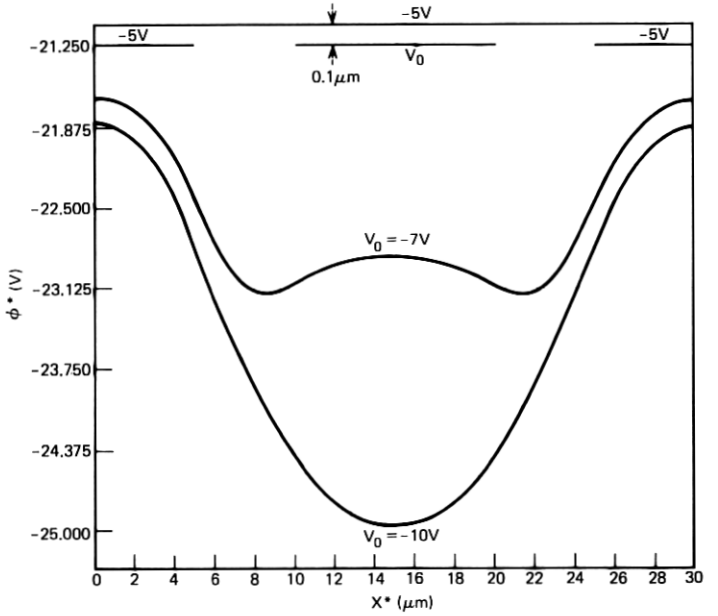

Fig. 9—The channel potential in the CCD of Fig. 7 with the separation of the metalization levels held fixed at $h^*_{-1} = 0.1$ μm and the potential of the center, lower-level electrode taking the values -7 and -10 V.

neighboring electrodes on the lower level will insure the absence of potential wells in the gaps.

In Fig. 9 we plot the channel potential for the same device but with $h^*_{-1} = 0.1$ μm and for $v_0 = -7$ and -10 V. For this small separation of the levels of metalization, a 5-V potential difference between neighboring electrodes eliminates potential wells in the gaps.

In Figs. 10 and 11 we show some effects of gap width. We consider first a buried channel CCD with double-level metalization. The p-layer is 5 μm thick ($h_2^* - h_1^* = 5$ μm), the oxide layer between the first level of electrodes and the p-layer is 0.1 μm thick ($h_1^* = 0.1$ μm), and the layer between the two levels of electrodes is 0.5 μm ($h^*_{-1} = 0.5$ μm). The upper level of electrodes consists of a single electrode at a potential of -5 V. The lower level consists of electrodes 10 μm wide and, as shown in Fig. 10, they are alternatively at potentials of -5 and -7 V. Curves of the channel potentials are plotted for three different gap widths between plates: 5, 1, and 0 μm. (The 0-gap curve was calculated by the methods of I.) The x^* scale for the three curves are different, but are chosen so the centers of the gaps coincide. With 5-μm-wide gaps,

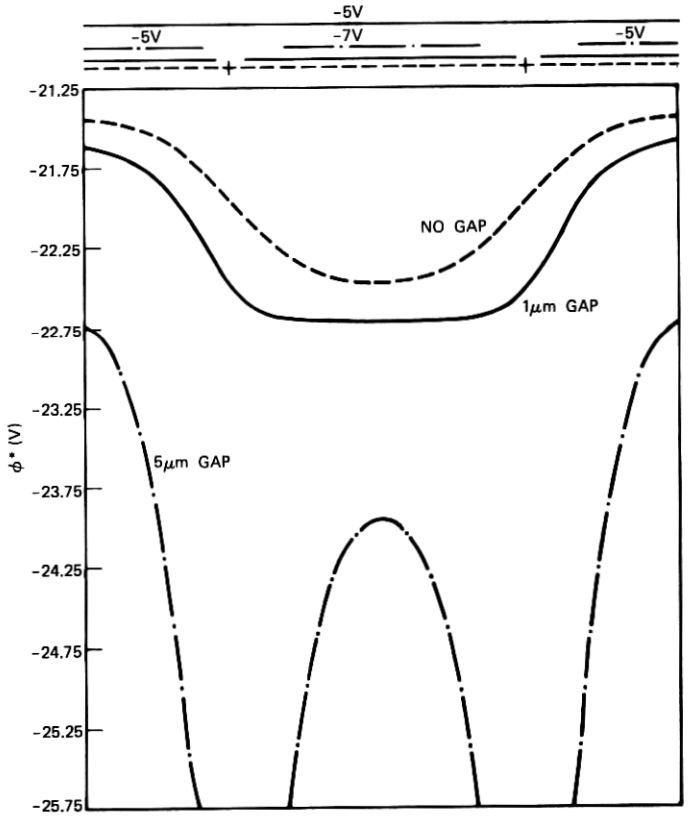

Fig. 10—The channel potential in the CCD of Fig. 7 with the separation of the metalization levels held fixed at $h^*_{-1} = 0.5$ μm, and the gap width taking the values 5, 1, and 0 μm.

there are large potential wells, as we saw in Figs. 7 and 8. However, by reducing the gap width to 1 μm, the potential wells are essentially eliminated. The curve for zero electrode separation is included to show that it is a good approximation to the channel potential in cases of small electrode separation.

Finally, in Fig. 11, we plot the potential along the oxide-semiconductor interface ($y^* = h_1^*$) for two surface CCD's. In each case, the oxide layer is 0.1 μm thick ($h_1^* = 0.1$ μm) and the region $y^* < 0$ is assumed to be filled with SiO_2. Also, in both cases, the electrodes are 10 μm wide and are held at alternate potentials of -5 and -7 V. In one case the gap between electrodes is 1 μm, while in the other case there are no gaps between electrodes. (The zero gap curve was calcu-

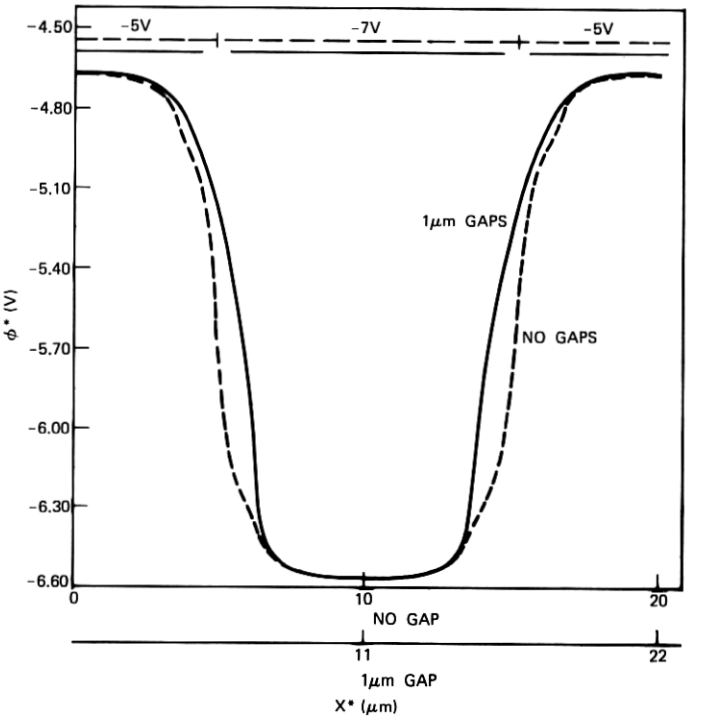

Fig. 11—The potential $\varphi^*(x^*, h_1^*)$ plotted as a function of x^* for a surface CCD with single-level metalization; $h_1^* = 0.1$ μm; 10-μm-wide electrodes held at -5 and -7 V; and with gaps between electrodes of 1 and 0 μm.

lated by the method of I.) Again the x^* scales differ, but the centers of the gaps coincide. Except in the region between the plates, the two curves coincide closely.

V. COMMENTS ON ACCURACY AND COST

We considered in some detail in I how well the solutions of the linearized equations (21) to (25) approximate the solutions of the nonlinear equations (7) to (10). It was shown there and in Ref. 4 that as long as $\max_{0 \leq x \leq L} \psi_1(x, h_1) \leqq -160$, and $|\psi_4(x, h_3) + 1| < 10, 0 \leqq x \leqq L$, [$|\psi_3(x, h_2) + 1| < 10$ for surface devices] then the solution of the linearized problem approximates the solution of the nonlinear problem to within several percent in the p-layer for buried channel devices (near the oxide-semiconductor interface for surface devices). In addition, we are interested in examining the accuracy of the approximate

solutions of the linearized equations. As we stated in Section III (and prove in Appendix B), the difference between the exact solution and the approximate solution, $\delta^*(x^*, y^*) = \psi^*(x^*, y^*) - \psi^{a*}(x^*, y^*)$, is bounded everywhere by its maximum value on the electrodes.

As typical examples, consider the curves in Figs. 10 and 11. For all three curves in Fig. 10, we found that $\psi_1(x, h_1) \leqq -345$ and $|\psi_4(x, h_2) + 1| < 2.75$ for $0 \leqq x \leqq L$. For the two curves of Fig. 11, we found that $\psi_1(x, h_1) < -186$ and $|\psi_3(x, h_2) + 1| \leqq 1$ for $0 \leqq x \leqq L$. Furthermore, for the curves of Fig. 10, a search of the electrodes showed that, for 5-μm gaps between electrodes, $\max |\delta^*(x^*, y^*)| \leqq 0.29$ V and, for 1-μm gaps, $\max |\delta^*(x^*, y^*)| \leqq 0.18$ V. (The no-gaps curve was calculated by the methods of I.) These correspond to maximum errors of the channel potential of 1.3 and 0.83 percent respectively. For the curve for the surface CCD with 1-μm gaps between the electrodes a search of the electrodes showed that $\max |\delta^*(x^*, y^*)| \leqq 0.4$ V. (The no-gaps curve was again calculated by the methods of I.) This corresponds to a maximum percentage error of 0.86 percent.

For the curves of the buried channel CCD of Fig. 10, we have undoubtedly overestimated the error in the channel for the following reasons. It can be shown that the error in each coefficient a_n and b_n appearing in (34) can be expressed as an integral over the electrodes of the error $\delta(x, y)$ times a weight function. The sign of $\delta(x, y)$ oscillates on the electrodes, and so one would expect the error in the lower-order coefficients to be quite small. Furthermore, an examination of (34) to (38) and (40) shows that, for the parameters involved, only the first ten terms in (40) contribute significantly to the channel potential.

To present some idea of the cost of running these programs, the calculation of the solution for the case of 5-μm gaps in the curves of Fig. 10 took 253 seconds and used 40 K of core, the case of 1-μm gaps took 258 seconds and 40 K of core. Calculation of the solution for the 1-μm gap case of Fig. 11 took 263 seconds and used 40 K of core. By comparison, the two corresponding no-gap solutions, obtained by the methods of I, took 16 seconds and 32 seconds, respectively, and both solutions required 40 K of core.

VI. ACKNOWLEDGMENTS

The authors take pleasure in thanking G. E. Smith for originally suggesting this research and for many subsequent conversations. They also benefitted from many conversations on the subject of CCD's with R. H. Krambeck, R. J. Strain, and R. H. Walden.

APPENDIX A

This appendix lists the coefficients of the Fourier series of the various splines used in approximating the charge density on the electrodes. We begin by defining the function

$$u(x, h) = \begin{cases} \left(1 - \frac{x}{h}\right), & 0 \leqq x \leqq h, \\ 0, & h \leqq x \leqq L. \end{cases} \tag{69}$$

Outside the interval $0 \leqq x \leqq L$, this function is defined by periodicity, $u(x, h) = u(x + L, h)$. The Fourier coefficients of $u(x, h)$ are

$$\begin{aligned} a_n(h) &= c_n[u] = \frac{2}{Lh\lambda_n^2}(1 - \cos \lambda_n h), \\ b_n(h) &= s_n[u] = \frac{2}{Lh\lambda_n^2}(\lambda_n h - \sin \lambda_n h), \end{aligned} \tag{70}$$

where the notation $c_n[u]$ and $s_n[u]$ is defined in (58), $\lambda_n = 2n\pi/L$, and $n = 0, 1, 2, \cdots$. Note that

$$a_0(h) = \frac{h}{L}, \qquad b_0(h) = 0. \tag{71}$$

The triangular splines can all be expressed in terms of $u(x, h)$, and their Fourier coefficients are simple linear functions of the coefficients $a_n(h)$ and $b_n(h)$ defined in eq. (70). Thus (see Fig. 4a):

$$p_0(x, h) = u(x, h) + u(L - x, h), \tag{72}$$

and for $n = 0, 1, 2, \cdots$,

$$c_n[p_0] = 2a_n(h), \qquad s_n[p_0] = 0. \tag{73}$$

Similarly (see Figs. 4b and 4c), we have the end splines

$$p_l(x; x_0, h) = u(x - x_0, h), \qquad p_r(x; x_0, h) = u(x_0 - x, h), \tag{74}$$

and for $n = 0, 1, 2, \cdots$

$$\begin{aligned} c_n[p_l] &= (\cos \lambda_n x_0)a_n(h) - (\sin \lambda_n x_0)b_n(h), \\ s_n[p_l] &= (\sin \lambda_n x_0)a_n(h) + (\cos \lambda_n x_0)b_n(h), \end{aligned} \tag{75}$$

and

$$\begin{aligned} c_n[p_r] &= (\cos \lambda_n x_0)a_n(h) + (\sin \lambda_n x_0)b_n(h), \\ s_n[p_r] &= (\sin \lambda_n x_0)a_n(h) - (\cos \lambda_n x_0)b_n(h). \end{aligned} \tag{76}$$

Finally (see Fig. 4f),

$$\begin{aligned} t(x; x_0, h_1, h_2) &= u(x_0 - x, h_1) + u(x - x_0, h_2), \quad x \not\equiv x_0 (\text{mod } L) \\ &= 1, \quad x = x_0 (\text{mod } L) \end{aligned} \tag{77}$$

and

$$\begin{aligned} c_n[t] &= \cos \lambda_n x_0 \{a_n(h_1) + a_n(h_2)\} + \sin \lambda_n x_0 \{b_n(h_1) - b_n(h_2)\}, \\ s_n[t] &= \sin \lambda_n x_0 \{a_n(h_1) + a_n(h_2)\} - \cos \lambda_n x_0 \{b_n(h_1) - b_n(h_2)\}. \end{aligned} \tag{78}$$

The coefficients of the Fourier series of the singular edge splines were calculated as follows. We define (see Figs. 4d and 4e)

$$s_\ell(x; x_0, h) = \begin{cases} = (x - x_0)^{-\frac{1}{2}} - h^{-\frac{1}{2}}, & x_0 < x \leqq x_0 + h, \\ = 0, & 0 \leqq x \leqq x_0, \quad x_0 + h < x \leqq L, \end{cases} \tag{79}$$

and

$$s_r(x; x_0, h) = s_\ell(2x_0 - x; x_0, h). \tag{80}$$

Then after an integration by parts

$$\begin{aligned} c_n[s_\ell] &= \\ &= \frac{4}{L}\left[h^{\frac{1}{2}} \cos \lambda_n (x_0 + h) - \frac{\sin \lambda_n (x_0 + h) - \sin \lambda_n x_0}{2\lambda_n h^{\frac{1}{2}}} \right. \\ &\qquad \left. + \lambda_n \int_{x_0}^{x_0+h} (x - x_0)^{\frac{1}{2}} \sin \lambda_n x dx \right], \end{aligned} \tag{81}$$

$$\begin{aligned} s_n[s_\ell] &= \\ &= \frac{4}{L}\left[h^{\frac{1}{2}} \sin \lambda_n (x_0 + h) + \frac{\cos \lambda_n (x_0 + h) - \cos \lambda_n x_0}{2\lambda_n h^{\frac{1}{2}}} \right. \\ &\qquad \left. - \lambda_n \int_{x_0}^{x_0+h} (x - x_0)^{\frac{1}{2}} \cos \lambda_n x dx \right]. \end{aligned}$$

The integrals on the right of (81) were evaluated by quadratures using Filon's method.[14] Similarly,

$$\begin{aligned} c_n[s_r] &= \\ &= \frac{4}{L}\left[h^{\frac{1}{2}} \cos \lambda_n (x_0 - h) - \frac{\sin \lambda_n x_0 - \sin \lambda_n (x_0 - h)}{2\lambda_n h^{\frac{1}{2}}} \right. \\ &\qquad \left. - \lambda_n \int_{x_0-h}^{x_0} (x_0 - x)^{\frac{1}{2}} \sin \lambda_n x dx \right], \end{aligned} \tag{82}$$

$$\begin{aligned} s_n[s_r] &= \\ &= \frac{4}{L}\left[h^{\frac{1}{2}} \sin \lambda_n (x_0 - h) + \frac{\cos \lambda_n x_0 - \cos \lambda_n (x_0 - h)}{2\lambda_n h^{\frac{1}{2}}} \right. \\ &\qquad \left. + \lambda_n \int_{x_0-h}^{x_0} (x_0 - x)^{\frac{1}{2}} \cos \lambda_n x dx \right]. \end{aligned}$$

APPENDIX B

We assume that a solution of equations (21) to (25) satisfying boundary and interface conditions (11) or (12) and (13) to (16), (18), (26), and (27) exists and is bounded. As before, we denote this solution by $\psi(x, y)$, we denote our approximate solution by $\psi^a(x, y)$, and we define

$$\xi(x, y) = \psi(x, y) - \psi^a(x, y). \tag{83}$$

By ψ_α, ψ^a_α, and ξ_α, $(0 \leqq \alpha \leqq 4)$, we mean ψ, ψ^a, and ξ restricted to the various subdomains.

From their construction, the approximate solutions satisfy the same equations and boundary and interface conditions as the exact solution, except they do not assume the correct values on the electrodes. Consequently

$$\nabla^2\xi_\alpha(x, y) = 0, \quad (0 \leqq \alpha \leqq 3), \quad \nabla^2\xi_4(x, y) - \xi_4(x, y) = 0. \tag{84}$$

Also $\xi_\alpha(x, y)$ satisfies either boundary condition (11) in the case of single-level metalization or

$$\xi_0(x, -h_{-1}) = 0 \tag{85}$$

in the case of double-level metalization. In addition, $\xi_0(x, 0) = \xi_1(x, 0)$, $0 \leqq x \leqq L$, and $\xi_\alpha(x, y)$ satisfies (14) with $\rho_\varrho \equiv 0$, (15) with $Q(x) \equiv 0$, (16), (18), (26), and (27).

We now outline a proof that if $M = \sup_{x \in E} |\xi_0(x, 0)|$, where E denotes the electrodes, then $|\xi(x, y)| \leqq M$ for all (x, y). The plan of the proof is to show that $\xi_0(x, y)$ is bounded both above and below by its maximum and minimum on $(0 \leqq x \leqq L, y = 0)$; that $\xi_\alpha(x, y)$ is bounded above and below by its maximum and minimum on either $(0 \leqq x \leqq L, y = h_{\alpha-1})$ or $(0 \leqq x \leqq L, y = h_\alpha)$, $(\alpha = 1, 2, 3)$, where we define $h_0 = 0$; and that $\xi_4(x, y)$ is bounded above and below by its maximum and minimum on $(0 \leqq x \leqq L, y = h_3)$. Then we show that the global maximum and minimum must occur on the electrodes.

First consider $\xi_0(x, y)$ in the case of single-level metalization. Then $\xi_0(x, y)$ is harmonic in the strip $S_0 = (0 \leqq x \leqq L, -\infty < y \leqq 0)$, and, by the Phragmen-Lindelöf theorem [Ref. 15, corollary to theorem 19, Chapter 2, with $w(x, y, = 1 - y]$, $\xi_0(x, y)$ is bounded in S_0, both above and below, by its values on the lines $(x = 0, -\infty < y \leqq 0)$, $(y \leqq x \leqq L, y = 0)$, and $(x = L, -\infty < y \leqq 0)$. Let $m_0 = \inf_{0 \leqq x \leqq L} \xi_0(x, 0)$ and $M_0 = \sup_{0 \leqq x \leqq L} \xi_0(x, 0)$. [Note that since $\xi(x, 0)$ is continuous, there exist points $0 \leqq x_m, x_M \leqq L$ such that $m_0 = \xi_0(x_m, 0)$, $M_0 = \xi_0(x_M, 0)$.]

Further, we must have

$$\xi_0(x, y) = \tfrac{1}{2}\beta_0 + \sum_{n=1}^{\infty} (\beta_n \cos \lambda_n x + \gamma_n \sin \lambda_n x) e^{\lambda_n y}, \tag{86}$$

and hence

$$\lim_{y \to -\infty} \xi_0(0, y) = \lim_{y \to -\infty} \xi_0(L, y) = \frac{1}{2}\beta_0 = \frac{1}{L}\int_0^L \xi_0(z, 0)\, dz. \tag{87}$$

From (87) we can conclude that

$$m_0 \leqq \lim_{y \to -\infty} \xi_0(0, y) = \lim_{y \to -\infty} \xi_0(L, y) \leqq M_0. \tag{88}$$

Now if M_0 is not the maximum value of $\xi_0(x, y)$, from what we have just shown, and from the periodicity of $\xi(x, y)$ in x, this maximum value must be assumed at two points $(0, y_0)$ and (L, y_0), with $-\infty < y_0 < 0$. Further, the outward directed normal derivative at these points must be positive (Ref. 15, theorem 8, Chapter 2); that is, $-(\partial \xi_0/\partial x)(0, y_0) > 0$, $(\partial \xi_0/\partial x)(L, y_0) > 0$. However, from periodicity, $(\partial \xi_0/\partial x)(0, y_0) = (\partial \xi_0/\partial x)(L, y_0)$, which is a contradiction. Hence M_0 is the maximum value of $\xi_0(x, y)$ in S_0. The same reasoning applied to $-\xi_0(x, y)$ shows that m_0 is the minimum value in S_0.

In the case of double-level metalization, the maximum principle for harmonic functions (Ref. 15, theorem 2, Chapter 2), plus the boundary condition $\xi_0(x, -h_{-1}) = 0$, implies that $\xi_0(x, y)$ is bounded everywhere in $(0 \leqq x \leqq L) \times (-h_{-1} \leqq y \leqq 0)$, both above and below, by its values on the sides $(x = 0, \ -h_{-1} \leqq y \leqq 0)$, $(0 \leqq x \leqq L, \ 0)$, and $(x = L, \ -h_{-1} \leqq y \leqq 0)$. Then the same reasoning as in single-level metalization shows that $\xi_0(x, y)$ achieves its maximum and minimum on $(0 \leqq x \leqq L, \ y = 0)$.

Essentially the same arguments used in the double-level metalization case can be used to show that $\xi_\alpha(x, y)$ $(\alpha = 1, 2, 3)$ must achieve both its maximum and minimum either on the line $(0 \leqq x \leqq L, \ y = h_{\alpha-1})$ or $(0 \leqq x \leqq L, \ y = h_\alpha)$, where we define $h_0 = 0$.

The Phragmen-Lindelöf theorem can be applied to $\xi_4(x, y)$ in $S_4 = (0 \leqq x \leqq L) \times (h_3 \leqq y < \infty)$ to show that $\xi_4(x, y)$ is bounded everywhere in S_4 both above and below by its values on $(x = 0, \ h_3 \leqq y < \infty)$, $(0 \leqq x \leqq L, \ y = h_3)$, and $(x = L, \ h_3 \leqq y < \infty)$. Making use of the boundary condition $\xi_4(x, \infty) = 0$, the same arguments used in the case of single-level metalization for $\xi_0(x, y)$ show that $\xi_4(x, y)$ achieves its maximum and minimum values on $(0 \leqq x \leqq L, \ y = h_3)$.

We have shown that $\xi(x, y)$ must assume its maximum and minimum values at points on the lines $(0 \leqq x \leqq L, \ y = h_\alpha)$, $0 \leqq \alpha \leqq 3$. Suppose

that $\xi(x, y)$ is a global maximum at the point $P = (z, h_\alpha)$. Then clearly $\psi_\alpha(x, y)$ and $\psi_{\alpha+1}(x, y)$ take on their maximum values at P. Consequently, their exterior normal derivatives at P must be positive (Ref. 15, theorem 8, Chapter 2), i.e., $(\partial\psi_\alpha/\partial y)(P) > 0$, $-(\partial\psi_{\alpha+1}/\partial y)(P) > 0$. However, if P is not a point on an electrode, it follows from interface conditions (14), (15) with $Q(x) = 0$, (16), or (26) that either $\eta(\partial\psi_\alpha/\partial y)(P) = (\partial\psi_{\alpha+1}/\partial y(P)$ or $(\partial\psi_\alpha/\partial y)(P) = (\partial\psi_{\alpha+1}/\partial y)(P)$, which is a contradiction. Consequently $\xi(x, y)$ achieves its maximum M_0 on an electrode. The same argument applied to $-\xi(x, y)$ shows that $\xi(x, y)$ also achieves its minimum m_0 on an electrode. If we set $M = \max(|m_0|, |M_0|)$, then we have shown that $|\xi(x, y)| \leqq M$.

REFERENCES

1. McKenna, J., and Schryer, N. L., "The Potential in a Charge-Coupled Device with No Mobile Minority Carriers and Zero Plate Separation," B.S.T.J., *52*, No. 5 (May-June 1973), pp. 669–696.
2. Boyle, W. S., and Smith, G. E., "Charge-Coupled Semi-Conductor Devices," B.S.T.J., *49*, No. 4 (April 1970) pp. 587–593.
3. Amelio, G. F., Tompsett, M. F., and Smith, G. E., "Experimental Verification of the Charge-Coupled Device Concept," B.S.T.J., *49*, No. 4 (April 1970), pp. 593–600.
4. McKenna, J., and Schryer, N. L., "On the Accuracy of the Depletion Layer Approximation for Charge-Coupled Devices," B.S.T.J., *51*, No. 7 (September 1972), pp. 1471–1485.
5. Walden, R. H., Krambeck, R. H., Strain, R. J., McKenna, J., Schryer, N. L., and Smith, G. E., "The Buried Channel Charge-Coupled Device," B.S.T.J., *51*, No. 7 (September 1972), pp. 1635–1640.
6. Boyle, W. S., and Smith, G. E., "Charge-Coupled Devices—A New Approach to MIS Device Structures," IEEE Spectrum, *8*, No. 7 (July 1971), pp. 18–27.
7. Grove, A. S., *Physics and Technology of Semiconductor Devices*, New York: John Wiley & Sons, 1967, pp. 49–50.
8. Krambeck, R. H., Walden, R. H., and Pickar, K. A., "A Doped Surface Two-Phase CCD," B.S.T.J., *51*, No. 8 (October 1972), pp. 1849–1866.
9. Schryer, N. L., "Constructive Approximation of Solutions To Linear Elliptic Boundary Value Problems," SIAM J. Num. Anal., *9*, No. 4 (December 1972), pp. 546–572. See references in this paper to further work along these lines.
10. Lehman, R. S., "Developments at an Analytic Corner of Solutions of Elliptic Partial Differential Equations," J. Math. Mech., *8*, No. 5 (September 1959), pp. 727–760.
11. Morrison, J. A., Cross, M. J., and Chu, T. S., "Rain-Induced Differential Attenuation and Differential Phase Shift at Microwave Frequencies," B.S.T.J., *52*, No. 4 (April 1973), pp. 599–604.
12. Elson, B. M., "Charge-Coupled Concept Studied for Photo-Sensors," Aviation Week and Space Technology, *96*, No. 21 (May 22, 1972), pp. 73–75.
13. Krambeck, R. H., "Zero Loss Transfer Across Gaps in a CCD," B.S.T.J., *50*, No. 10 (December 1971), pp. 3169–3175.
14. Filon, L. N. G., "On a Quadrature Formula For Trigonometric Integrals," Proc. Roy. Soc. Edin., *49* (1928–29), pp. 38–47.
15. Protter, M. H., and Weinberger, H. F., *Maximum Principles in Differential Equations*, Englewood Cliffs, N. J.: Prentice-Hall, 1967.